MATERIALS CHEMISTRY
FRONTIERS

RESEARCH ARTICLE

View Article Online
View Journal | View Issue

Check for updates

Cite this: *Mater. Chem. Front.*, 2019, **3**, 93

Pyrene-fused PDI based ternary solar cells: high power conversion efficiency over 10%, and improved device thermal stability†

Yanbin Gong,‡[a] Kai Chang,‡[a] Cheng Chen,[a] Mengmeng Han,[a] Xuejun Zhan,[a] Jie Min,*[b] Xuechen Jiao,[cd] Qianqian Li[a] and Zhen Li*[ae]

Received 24th September 2018,
Accepted 28th October 2018

DOI: 10.1039/c8qm00486b

rsc.li/frontiers-materials

Although great advances have been achieved in the field of organic solar cells (OSCs) with the rapid development of nonfullerene acceptors (NFAs), devices with simultaneous high power conversion efficiency (PCE) and thermal stability remain a big challenge, particular small molecule NFA-based devices. In this paper, we designed and synthesized a class of pyrene-fused perylene diimides (PDIs) for fabricating ternary OSCs, which exhibited much better device performance than those of the parent PDI counterpart based devices due to the better miscibility and crystallization of the ternary films. Excitingly, Th-PYPDI and O-PYPDI based ternary OSCs showed improved thermal stability, as a result of the better morphology stability under the same annealing conditions. Notably, the O-PYPDI based ternary device exhibited the best PCE of 10.96% and good thermal stability with the PCE remaining at 82% of the initial value after thermal annealing at 80 °C for 72 h.

Published on 29 October 2018. Downloaded by Fail Open on 7/23/2025 8:45:14 AM.

Introduction

Impressive progress has been made in the field of solution-processed bulk heterojunction (BHJ) organic solar cells (OSCs) with the highest power conversion efficiency (PCE) of 17.3%, revealing their potential prospects of promising and low-cost renewable energy.[1] The prerequisite to achieve high PCEs and stable device performance is to screen well matched donors (D) and acceptors (A) of the active layer, which is the most important part of cell devices.[2] In earlier studies, numerous polymer donors were designed and synthesized to blend together with fullerene acceptors (FAs) for the fabrication of OSC devices.[3] However, some drawbacks hampered the commercial process seriously, such as high cost, weak absorption in the visible region, limited energy-level tunability and so on.[4] Fortunately, great efforts have been made toward the development of nonfullerene acceptors (NFAs), leading to higher open-circuit voltage (V_{OC}), larger photocurrent and correspondingly much higher PCEs than those of FA-OSCs, thanks to their advantages of tunable energy level and better absorption.[5] Nowadays, research on small molecular NFAs has stimulated a new development of this field to some degree.[1a–c] To construct highly efficient NFAs, perylene diimide (PDI) is one of the most investigated electron-withdrawing building units due to its appropriate energy level, strong absorption, high mobility and excellent photochemical and thermal stability.[6] Yan's group reported a PDI-NFA with upshifting lowest unoccupied molecular orbital (LUMO) level, and a high V_{OC} exceeding 1.1 V was realized and the highest PCE reached 10.58%.[7] In our previous work, we reported two pyrene-fused PDI-NFAs, which exhibited moderate PCEs but an ultrahigh V_{OC} of 1.26 V.[8] This inspired us to develop more pyrene-fused PDI-NFAs with high V_{OC}.

Generally, the active layer can be classified into binary and ternary blends. Binary blends are made of D_1 and A_1, while D_2 or A_2 blends together with a binary system to form a ternary blend. Relatively, ternary OSCs can improve the performance of OSCs owing to their extended light absorption range and better photovoltaic properties rather than their binary counterparts.[9] Accordingly, numerous ternary devices have been fabricated to explore material combinations with high performance. However, the literature reports concerning PDI-NFA based ternary OSCs are very scarce regardless of the possible significance.[10] Recently, ternary OSCs exhibited that a second acceptor with higher V_{OC} could be mixed into a host binary blend solution to improve V_{OC} gradually with the increasing content of the second acceptor.[1a,10c,11] Thus, it should be very meaningful to fabricate ternary OSCs by utilizing our pyrene-fused PDI-NFAs, possibly resulting in the improvement of the device V_{OC}.

[a] *Department of Chemistry, Hubei Key Lab on Organic and Polymeric Opto Electronic Materials, Wuhan University Wuhan, 430072, China. E-mail: lizhen@whu.edu.cn, lichemlab@163.com; Fax: +86-27-68755767*
[b] *The Institute for Advanced Studies, Wuhan University, Wuhan 430072, China. E-mail: min.jie@whu.edu.cn*
[c] *Department of Materials Science and Engineering, Monash University, Victoria, Australia*
[d] *Australian Synchrotron, ANSTO, Clayton, Victoria, 3168, Australia*
[e] *Institute of Molecular Aggregation Science, Tianjin University, Tianjin 300072, China*
† Electronic supplementary information (ESI) available. See DOI: 10.1039/c8qm00486b
‡ These authors contributed equally to this work.

Published on 29 October 2018. Downloaded by Fail Open on 7/23/2025 8:45:14 AM.

According to the above considerations, in this paper, three pyrene-fused PDI-NFAs were rationally designed, while their PDI counterparts were also synthesized for comparison (Scheme S1 in the ESI†). These six NFAs were intermixed together with a mature host binary system of J71 and ITIC, to investigate their ternary OSC performance. As expected, the V_{OC} of the ternary OSCs increases gradually along with the increasing content of pyrene-fused PDI-NFAs, as a result of the varied organic alloy states. Notably, pyrene-fused PDI-NFA based devices exhibit much better performance than their PDI counterparts with the same incorporation content, due to the overall enhanced V_{OC}, short circuit current density (J_{SC}) and fill factor (FF). The J71 : ITIC : O-PYPDI (1 : 0.9 : 0.1) device exhibits the best performance with a PCE of 10.96%, a V_{OC} of 0.945 V, a J_{SC} of 16.59 mA cm^2 and an FF of 69.92%, which is comparable to that of the host binary device. Meanwhile, it should be highlighted that 10% content of O-PYPDI based ternary devices shows improved (about 10%) thermal stability compared to that of the host binary device, thanks to the higher morphology stability under the same annealing conditions. Thus, the obtained experimental results demonstrate that pyrene-fused PDI-NFAs are good candidates for fabricating ternary OSC devices, due to the complementary absorption in the short wavelength region, high V_{OC} and the ability to improve the thermal stability of ternary devices.

Results and discussion

Synthesis and characterization

The chemical structures of all pyrene-fused PDI-NFAs are depicted in Scheme 1. The target six NFAs, TPDI, Th-PDI, O-PDI, TPYPDI, Th-PYPDI and O-PYPDI were synthesized *via* a Stille coupling reaction with high yields (Scheme 1). The important intermediates of **1** and **2** were prepared according to the previous work of our group and three bis(trimethylstannyl) reagents were obtained from a commercial route.[12] All of the six NFAs were characterized by ^{1}H and ^{13}C NMR, and matrix-assisted laser desorption/ionization time of flight mass spectrometry (MALDI-TOF MS) analyses. Thanks to the long alkyl side chains, these six NFAs show very good solubility in common organic solvents such as chloroform, dichloromethane (DCM) and toluene, ensuring the easy fabrication of the solution-processed OSC devices. Their thermal stability was investigated by using thermogravimetric analysis (TGA) (Fig. 1a). TPDI, TPYPDI, Th-PDI and Th-PYPDI show excellent thermal stability with decomposition temperatures (T_d, 5% weight loss) of 463.1 °C, 450.7 °C, 460.9 °C and 423.2 °C, respectively. O-PDI and O-PYPDI were also thermally stable with relatively low T_d values of 356.6 °C and 362.4 °C, respectively.

Cyclic voltammetry (CV) measurements were performed to investigate the energy levels of the synthesized NFAs. As shown in Fig. S2 (ESI†), O-PYPDI displayed two reversible reduction waves, while only one for the other five NFAs. The LUMO energies of the six NFAs estimated from their onset reduction potentials were approximately −3.57 eV to −3.80 eV (Fig. 1b). Combined with the optical bandgaps, their HOMO energy levels were calculated to be in the range of −5.43 to −5.46 eV. Notably, in comparison with three parent PDIs, three pyrene-fused PDIs show significantly upshifted LUMO and highest occupied molecular orbital (HOMO) levels, due to the electron-donating effect of the pyrene unit. According to the literature reports, a higher LUMO energy level could result in a much larger offset between the HOMO of the donor polymer (J71, −5.40 eV)

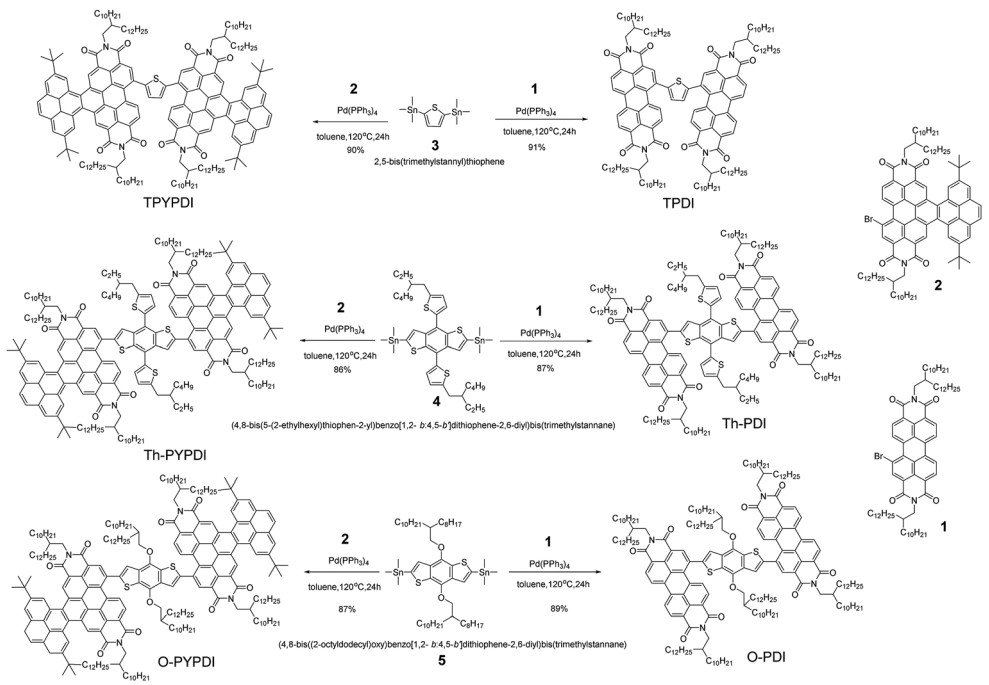

Scheme 1 Synthetic routes of the six NFAs.

 This journal is © The Royal Society of Chemistry and the Chinese Chemical Society 2019

Published on 29 October 2018. Downloaded by Fail Open on 7/23/2025 8:45:14 AM.

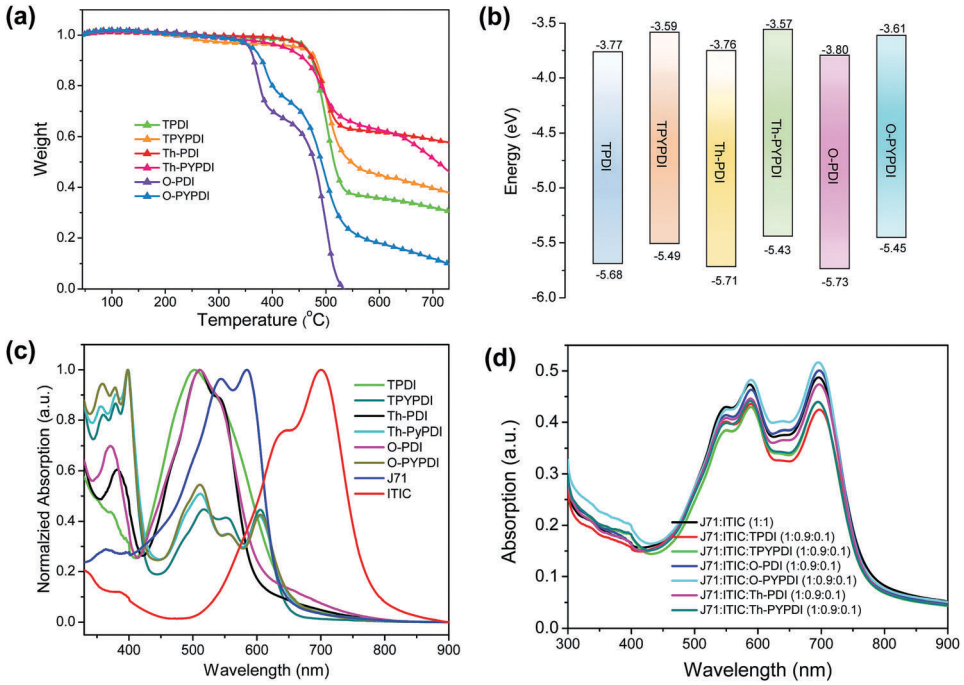

Fig. 1 (a) TGA curves of the synthesized six NFAs recorded under N_2 at a heating rate of 10 °C min^{-1}. (b) Energy level diagram of the synthesized six NFAs. (c) Absorption of each pure ternary active layer material in thin films. (d) Absorption spectra of J71:ITIC binary film and 10% content NFA based ternary films.

and the LUMO of the acceptor, and thus, a high V_{OC} could be anticipated.[7,8,10b]

The UV-vis absorption spectra of the six NFAs in chloroform solution and as films were measured (Fig. S1 in the ESI† and Fig. 1c). The absorptions in films show broader and redshifted absorption, in comparison with their solutions. In films, the three PDI-NFAs show similar absorption located at 400–600 nm. After ring-fusion with pyrene, the absorption edges redshifted relative to their PDI counterparts, due to the enlarged molecular conjugation. Interestingly, the most intense absorption band of the three pyrene-fused PDI NFAs located at 300–400 nm, while the relatively weak absorption band was from 450 to 650 nm, in which, the absorption peak at approximately 605 nm should be attributed to the intramolecular charge transfer caused by the ring-fusion with pyrene. As shown in Fig. 2b, the absorption spectrum of J71-ITIC film covers a broad absorption range from 300 nm to 900 nm, and there is an apparent weak absorption band from 300 to 450 nm. Thus, it is really very good that this weak absorption band could be enhanced by the incorporation of three pyrene-fused PDI-NFAs (Fig. 1d). The optical bandgaps of

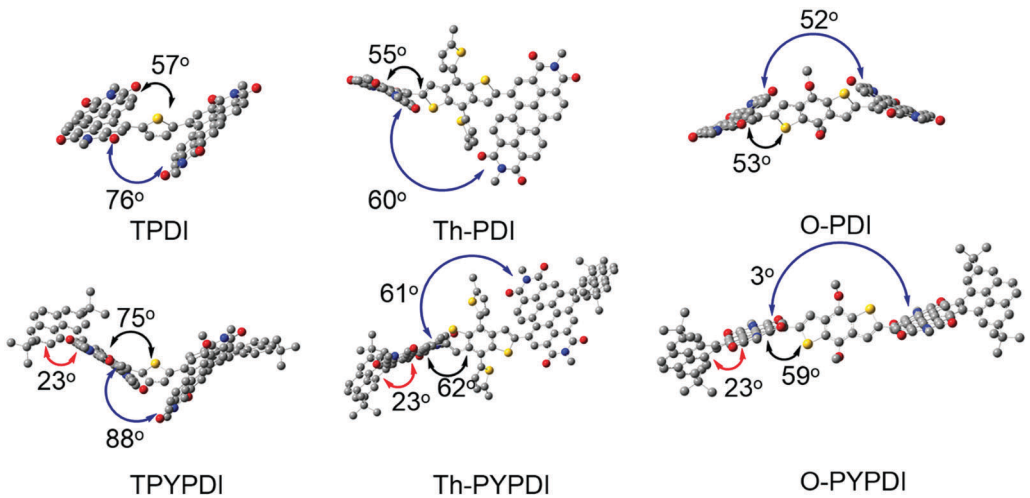

Fig. 2 The optimal geometries of TPDI, Th-PDI, O-PDI, TPYPDI, Th-PYPDI and O-PYPDI calculated by the Gaussian09 program at the B3LYP/6-31G level. Yellow S, gray C, red O, blue N.

Published on 29 October 2018. Downloaded by Fail Open on 7/23/2025 8:45:14 AM.

Table 1 Properties of the synthesized six NFAs

Compound	T_d[a] (°C)	$\lambda_{max,onset}$[b] (nm)	ε_{max}[c] (M^{-1} cm^{-1})	E_g[d] (eV)	E_{LUMO}[e] (eV)	E_{HOMO}[f] (eV)	$\lambda_{max,abs}$ Solv.[g] (nm)	$\lambda_{max,abs}$ Film[h] (nm)
TPDI	463.1	649	0.66×10^5	1.91	−3.77	−5.68	528	502
TPYPDI	450.7	653	1.20×10^5	1.90	−3.59	−5.49	397	399
Th-PDI	460.9	636	0.70×10^5	1.95	−3.76	−5.71	528	511
Th-PYPDI	423.2	667	1.34×10^5	1.86	−3.57	−5.43	397	399
O-PDI	356.6	642	0.71×10^5	1.93	−3.80	−5.73	528	511
O-PYPDI	362.4	674	1.26×10^5	1.84	−3.61	−5.45	397	398

[a] Five percent weight loss temperature measured by TGA under N_2. [b] Observed from the absorption spectra in the films. [c] Molar extinction coefficient at λ_{max} in solution. [d] Bandgap estimated from the optical absorption band edges of the films. [e] Calculated from the onset reduction potentials of the compounds. [f] Estimated using empirical equations $E_{HOMO} = E_{LUMO} - E_g$. [g] Absorption maximum in chloroform solution. [h] Absorption maximum in films.

these six NFAs were calculated to be in the range of 1.84–1.95 eV from the absorption edge. Compared to PDI NFAs, pyrene-fused PDI NFAs have a slightly narrow bandgap induced by larger π-conjugation, possibly leading to the decreased energy loss. The decomposition temperatures and basic photophysical properties of the six NFAs are summarized in Table 1.

Theoretical calculations

The optimized geometries of each parent PDI and pyrene-fused PDI were calculated by density functional theory (DFT) using Gaussian at the B3LYP/6-31G level (Fig. 2). The dihedral angles between the central donor and PDI are 57°, 55°, and 52° for TPDI, Th-PDI and O-PDI, respectively. Meanwhile, the dihedral angles between two PDI subunits decrease from 76°, to 60° to 53° for TPDI, Th-PDI and O-PDI, respectively. These observations suggest that the overall planarity of the molecular geometry was gradually increased with decreasing the steric hindrance of the central donor. Similarly, as the steric hindrance of the central donor decreases, the planarity of the pyrene-fused PDIs increases gradually. Additionally, the twist angles between pyrene and adjacent PDI are 23° for the three pyrene-fused PDIs. Notably, the overall geometry of O-PYPDI exhibits highly planarity with an almost parallel arrangement (3°) between two PDI subunits. Furthermore, the electron distribution of frontier orbitals was also affected by the pyrene fusing through adjusting LUMO and HOMO delocalization over the whole π-system (Fig. S3, ESI†). The LUMO levels of TPDI, Th-PDI, O-PDI, TPYPDI, Th-PYPDI and O-PYPDI were calculated to be −3.57, −3.50, −3.54, −3.23, −3.15 and −3.19 eV, respectively. And the calculated LUMO levels of pyrene-fused PDIs are higher than those of PDI counterparts, in agreement with the experimental results.

Photovoltaic properties

J71:ITIC was chosen as the host binary system and blended with the synthesized NFAs together to explore the ternary OSC performance. On one hand, ITIC is a famous NFA and industrially relevant developed by Zhan's group, which has been fully investigated to fabricate OSC devices with many polymer donors with PCEs surpassing 10%.[13] On the other hand, J71 is an efficient polymer donor and commercially available.[14] The binary OSCs based on J71:ITIC exhibit PCEs surpassing 11% with simultaneously high V_{OC} and high short circuit current density (J_{SC}). In addition, the solvent additive is not required to achieve the best device performance in the J71-ITIC system, which emphasizes the impact of ternary film morphology on other factors rather than solvent additive.

As shown in Fig. S4a (ESI†), all the OSC devices in this study were fabricated with a forward configuration of ITO/PEDOT:PSS/Active Layer/PDINO/Al and all the device parameters from ten devices are listed in Table S1 (ESI†). For ITIC:J71 based binary OSCs, a PCE of 11.08% was achieved with a V_{OC} of 0.939 V, a J_{SC} of 17.55 mA cm^{-2}, and a FF of 67.28%, which is comparable to that reported in the literature (≈11.4%).[14] However, J71:PDI-NFAs based binary OSCs showed poor PCEs (0.36–0.47%) with lower V_{OC} (0.652–0.833 V), J_{SC} and fill factor (FF). For J71:pyrene-fused PDI-NFAs based binary OSCs, the PCEs (0.37–1.47%) were slightly higher than that of J71:PDI-NFAs based binary OSCs, mainly due to the improved V_{OC} (1.013–1.047 V) derived from the upshifting LUMO energy level of pyrene-fused PDI-NFAs. As expected, the pyrene-fused PDI exhibited significantly improved V_{OC} than that of the parent PDI counterparts. However, the weak J_{SC} (1.26–4.22 mA cm^{-2}) led to the limited PCEs of J71:pyrene-fused PDI-NFA binary devices severely, partially caused by the blue shift of the main absorption band (300–400 nm). Based on the special properties of pyrene-fused PDI-NFAs, it can be used as a second acceptor to fabricate ternary OSCs and improve the V_{OC} as well as the absorption in the short wavelength region of ternary devices.

Ternary active layers of J71:ITIC:NFAs with various NFA contents were blended together, where the NFAs were three target parent PDIs and three pyrene-fused PDIs. The overall ratio of donor to acceptor was kept at 1 : 1 in this study. According to the device performance of J71:ITIC:NFAs with different NFA content (Table S1 in the ESI†), 10% was chosen as the optimal content to explore the influence of the addition of second NFAs on the absorption, film morphology, device performance and thermal stability of J71:ITIC:NFA ternary devices. Current density–voltage (*J*–*V*) characteristics of the best-performing devices are shown in Fig. 3a–c, while the corresponding external quantum efficiency (EQE) spectra are demonstrated in Fig. 3d–f, with the best-performing device parameters summarized in Table 2. The J71 : ITIC : O-PYPDI (1 : 0.9 : 0.1) device exhibits the best performance with a PCE

 This journal is © The Royal Society of Chemistry and the Chinese Chemical Society 2019

Published on 29 October 2018. Downloaded by Fail Open on 7/23/2025 8:45:14 AM.

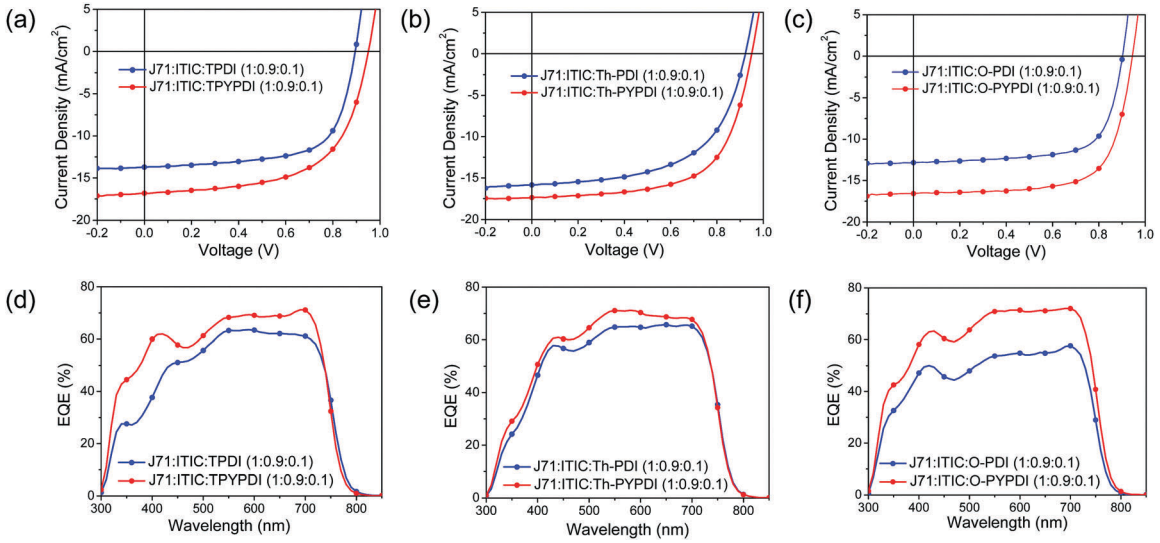

Fig. 3 *J*–*V* curves and corresponding EQE spectra of J71:ITIC:NFAs ternary OSC devices.

Table 2 Summary of device parameters of 10% content NFA based ternary OSC devices

Devices	V_{OC} [V]	J_{SC} [mA cm^{-2}]	FF [%]	PCE[a] [%] Best	Average
J71 : ITIC : TPDI (1 : 0.9 : 0.1)	0.913	13.55	62.03	7.67	7.34
J71 : ITIC : TPyPDI (1 : 0.9 : 0.1)	0.951	15.54	66.27	9.8	9.52
J71 : ITIC : Th-PDI (1 : 0.9 : 0.1)	0.93	15.23	62.82	8.91	8.71
J71 : ITIC : Th-PyPDI (1 : 0.9 : 0.1)	0.955	16.66	65.34	10.63	10.42
J71 : ITIC : O-PDI (1 : 0.9 : 0.1)	0.916	11.96	59.46	6.46	6.46
J71 : ITIC : O-PyPDI (1 : 0.9 : 0.1)	0.945	16.59	69.92	10.96	10.71
J71 : ITIC (1 : 1)	0.939	17.55	67.28	11.08	10.83

[a] The values are calculated from the statistical values from ten devices.

of 10.96%, a V_{OC} of 0.945 V, a J_{SC} of 16.59 mA cm^2 and an FF of 69.92%, which is comparable to that of the host binary device. Notably, the addition of PDI-NFAs yielded declined PCEs (6.46–8.91%), while the addition of pyrene-fused PDI-NFAs improved the PCEs (9.80–10.96%) with overall enhanced V_{OC}, J_{SC} and FF.

It is a clear trend that the V_{OC} of ternary OSCs increases gradually along with the content of pyrene-fused PDI-NFAs. On one hand, pyrene-fused PDI-NFAs have higher LUMO energy levels than that of ITIC, which gives a larger offset energy referencing to the HOMO of the donor material. On the other hand, ITIC and pyrene-fused PDI-NFAs could form close contact mixtures or new electronic alloys, leading to tunable V_{OC}s in ternary OSCs caused by the charge transfer state.

Compared to PDI-NFAs, the increased J_{SC}s of pyrene-fused PDI-NFA based devices are consistent with comparable changes in the corresponding EQE spectra, which should be partially originated from the enhanced absorption of pyrene-fused PDI-NFAs and improved charge separation or collection. As shown in Table 2, the J_{SC} of the J71:ITIC binary device is 17.55 mA cm^{-2}, meanwhile the J_{SC} is 15.54, 16.66 and 16.59 mA cm^{-2} for J71 : ITIC : TPYPDI (1 : 0.9 : 0.1), J71 : ITIC : Th-PYPDI (1 : 0.9 : 0.1), and J71 : ITIC : O-PYPDI (1 : 0.9 : 0.1), respectively. Thus, the 10% content incorporation of pyrene-fused PDI-NFAs resulted in a small decrease, which should be derived from two aspects. On one hand, pyrene is a good hole transport molecule, and thus the ring-fusion with pyrene would decrease the electron transport mobility of pyrene-fused PDI derivatives, resulting in the low J_{SC}. In our previous and this work, we reported five pyrene-fused PDI-NFAs, all of which exhibited low J_{SC} ($<$6.83 mA cm^{-2}) in the binary devices. On the other hand, by replacing 10% content of ITIC with pyrene-fused PDI-NFAs, the absorption at 300–400 nm increased with the sacrifice of absorption at 650–800 nm, leading to a possible small decrease of the overall absorption in the visible region. Taking these two aspects together, the J_{SC} of J71 : ITIC : pyrene-fused PDI-NFA (1 : 0.9 : 0.1) devices exhibited a small decrease.

In comparison with PDI-NFAs, the enhanced FF of pyrene-fused PDI-NFA based OSC devices may be connected with the charge mobility and film morphology, which will be discussed in the following sections.

Hole and electron mobilities of J71 : ITIC : NFAs (1 : 0.9 : 0.1) ternary devices were measured using the space charge limited current (SCLC) method. The structure of the hole only devices was Glass/ITO/PEDOT:PSS/Active Layer/MoO*x*/Ag. As for electron only devices, the structure was Glass/ITO/ZnO/Active Layer/Ca/Al. The hole mobilities range from 0.92 $\times$ 10^{-3} (10 wt% TPDI) to 2.84 $\times$ 10^{-3} cm^2 V^{-1} s^{-1} (10 wt% O-PYPDI), while the electron mobilities are in the range of 1.02 $\times$ 10^{-3}–2.39 $\times$ 10^{-3} cm^2 V^{-1} s^{-1} (10 wt% O-PYPDI), with the μ_h, μ_e and μ_h/μ_e values presented in Table S2 (ESI†). Notably, the μ_h/μ_e values in these pyrene-fused PDI-NFA based devices were more balanced, in comparison with those of their corresponding parent PDI-NFA based devices (from 0.49 to 1.27, 1.68 to 0.80, and 1.60 to 1.19). The more balanced μ_h/μ_e contributes to the higher FF of pyrene-fused PDI-NFA based devices, and the highest FF value (69.92%) of the O-PYPDI based device results from the simultaneously higher mobility and more balanced μ_h/μ_e.

Published on 29 October 2018. Downloaded by Fail Open on 7/23/2025 8:45:14 AM.

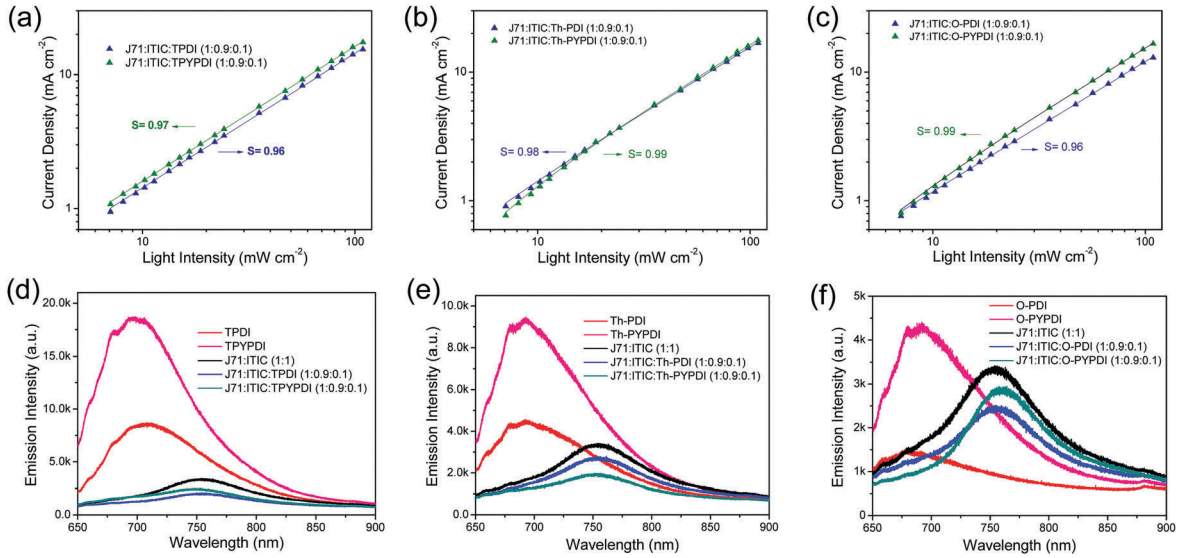

Fig. 4 Light intensity dependent photocurrent experiments of J71:ITIC:TPDI and J71:ITIC:TPYPDI films (a), J71:ITIC:Th-PDI and J71:ITIC:Th-PYPDI films (b), and J71:ITIC:O-PDI and J71:ITIC:O-PYPDI films (c). Photoluminescence quenching spectra of neat films, J71:ITIC binary film and corresponding ternary films of TPDI and TPYPDI (d), Th-PDI and Th-PYPDI (e), and O-PDI and O-PYPDI (f). PL excitation of the films was at 532 nm.

To investigate the charge recombination in the J71 : ITIC : NFA (1 : 0.9 : 0.1) ternary devices, measurements of light intensity dependent J_{SC} were conducted. J_{SC} as a function of incident light intensity (P) is described in Fig. 4a, b and c, respectively. The relationship between J_{SC} and P can be expressed as $J_{SC} \propto P^S$. The bimolecular recombination can be neglected in ternary films, if the S value is close to 1. The fitted S values are approximately 0.96, 0.97, 0.98, 0.99, 0.96 and 0.99 for the TPDI, TPYPDI, Th-PDI, Th-PYPDI, O-PDI and O-PYPDI based ternary active layers, respectively, suggesting that bimolecular recombination was hardly observed in ternary devices with the incorporation of 10% NFAs. Considering that the fitted S values of the pyrene-fused PDI-NFA based devices were slightly closer to 1 rather than those of the PDI counterpart based devices, the bimolecular recombination can be slightly suppressed in the devices of J71 : ITIC : pyrene-fused PDI-NFAs (1 : 0.9 : 0.1) compared to J71 : ITIC : PDI-NFAs (1 : 0.9 : 0.1).

To confirm the energy transfer in the donor–acceptor interface, the photoluminescence (PL) quenching measurements were carried out. As shown in Fig. S6 (ESI†), the neat films of both J71 and ITIC exhibit broad emission bands, with the peaks at 695 and 765 nm, respectively. The emission peak in the J71:ITIC binary film red shifted to 750 nm with a PL quenching efficiency of 0.82 as compared to the respective neat J71 film, indicating conspicuous energy transfer in the J71-ITIC interface. The PL spectra of neat films of each pure NFA and the corresponding ternary films are shown in Fig. 4d–f, and the pyrene-fused PDI-NFA neat films exhibit much stronger PL intensity compared to those of PDI counterpart neat films. Notably, with the incorporation of 10% content of NFAs in ternary films, the PL quenching efficiencies were improved to 0.89, 0.87, 0.85, 0.90, 0.87 and 0.85 for TPDI, TPYPDI, Th-PDI, Th-PYPDI, O-PDI and O-PYPDI, respectively, indicating the better energy transfer in the 10% content NFA based ternary films relative to the J71:ITIC binary film.

Film morphology

Atomic force microscopy (AFM) was used to study the morphology of the host binary and corresponding 10% content of NFA based ternary blend films. As shown in Fig. S7 (ESI†), the root-mean-square (RMS) roughness of the J71:ITIC binary film is 0.59 nm, indicating a smooth and uniform surface. When 10% content of ITIC was changed to pyrene-fused PDI-NFAs, the RMS roughnesses declined to 0.55, 0.57 and 0.57 nm for TPYPDI, Th-PYPDI and O-PYPDI, respectively. In contrast, by replacing 10% content of ITIC with PDI-NFAs, the RMS roughnesses increased to 0.70, 0.62 and 0.76 nm for TPDI, Th-PDI and O-PDI, respectively. Notably, large domains can be easily observed in J71 : ITIC : PDI-NFAs (1 : 0.9 : 0.1) ternary blend films, since PDI derivatives are known to aggregate severely.[7] The results revealed that the addition of 10% content of pyrene-fused PDI-NFAs is in favor of better miscibility of the ternary blend, whereas PDI NFAs tend to deteriorate the film morphology more or less.

It is an accepted notion that materials with a similar surface energy lead to close contact.[10c,15] The smaller the difference in surface energy is, the better the miscibility. Thus, to gain deeper insight into the miscibility of the ternary films, the contact angle and surface energy of the used materials were investigated. First, the contact angle measurements on thin films of each pure NFA were performed using two different liquids (water, ethylene glycol (EG)), to obtain two pairs of contact angles for each NFA. The surface energy of each pure NFA was calculated directly by instruments using the model of Wu.[16] As shown in Fig. 5b, the surface energy of J71 (22.0 mN m^{-1}) is similar to that of ITIC (24.1 mN m^{-1}), and the small surface energy difference (2.1 mN m^{-1}) between J71 and ITIC reveals their

 This journal is © The Royal Society of Chemistry and the Chinese Chemical Society 2019

Published on 29 October 2018. Downloaded by Fail Open on 7/23/2025 8:45:14 AM.

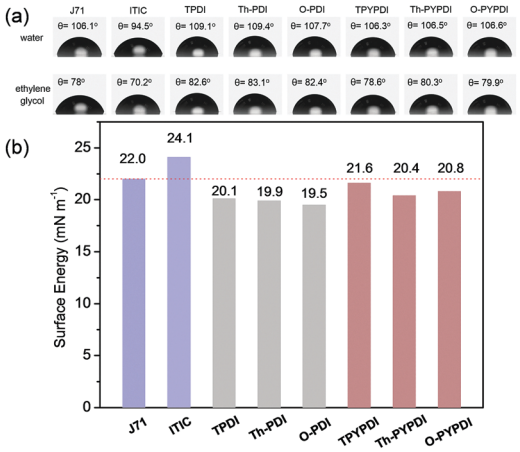

Fig. 5 (a) Contact angle images and contact angle value of the pure materials used in this work. (b) Surface energy of the pure materials used in this work.

close contact and good miscibility in films, which corresponds well to the AFM result of the binary film. Compared to the binary film of J71-ITIC, it should be highlighted that the surface energy difference between pyrene-fused PDI-NFAs and J71 is smaller (0.4, 1.6 and 1.2 mN m^{-1} for TPYPDI, Th-PYPDI and O-PYPDI, respectively). Thus, in comparison with the binary film, better miscibility can be obtained in the pyrene-fused NFA based ternary films. In contrast, PDI-NFAs exhibit larger surface energy difference with ITIC and J71, compared to that of pyrene-fused PDI counterparts, indicating the worse miscibility in PDI-NFA based ternary films. The results also explain the AFM profiles aforementioned well.

Grazing incidence wide angle X-ray scattering (GIWAXS) measurements were employed to characterize the molecular packing and crystallinity of the neat and blended films. As shown in Fig. S10 (ESI†), in the horizontal (in-plane) direction, the neat films of O-PDI show strong lamellar molecular packing with visible (200) and (300) peaks and a sharp (400) peak, indicating a dominant face-on orientation for better electron transport. In the similar diffraction vector (q) value, the slightly lower peaks were observed in the neat film of Th-PDI. In contrast, the (300) and (400) peaks almost disappeared in the neat film of TPDI. Such a trend of decreased in-plane lamellar packing in the neat film of PDI-NFAs should result from the planarity of the whole molecules. The same trend also exists in the neat film of

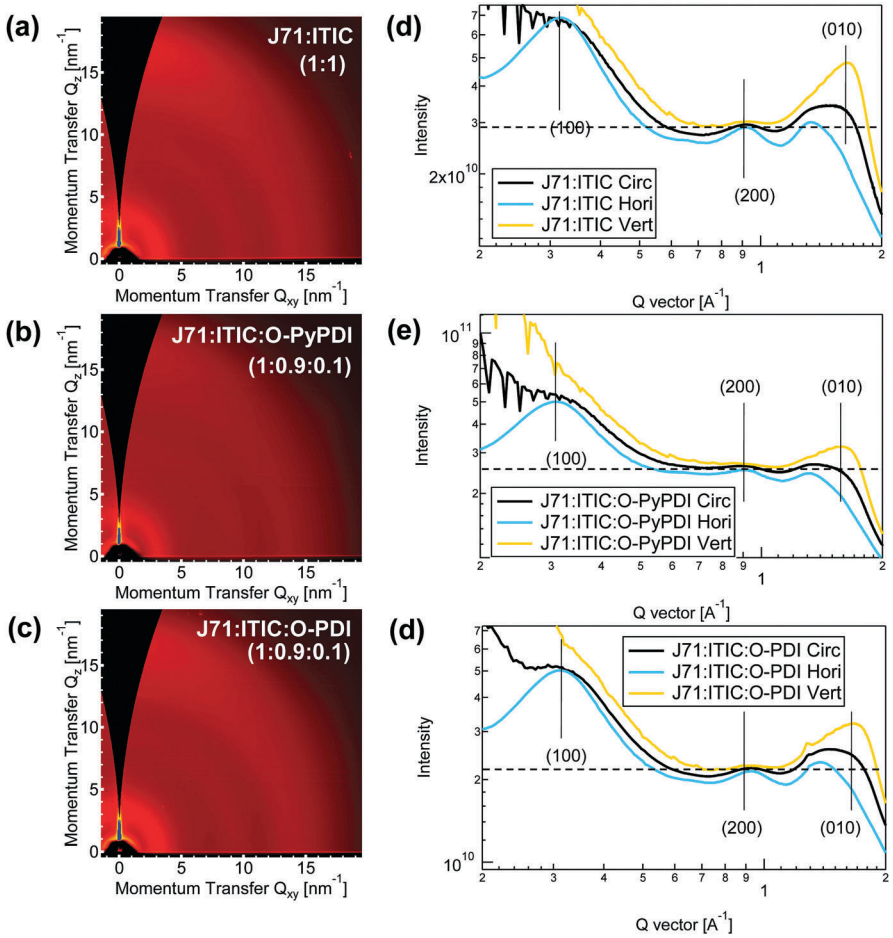

Fig. 6 GIWAXS patterns of J71:ITIC binary film (a), J71 : ITIC : O-PYPDI (1 : 0.9 : 0.1) ternary film (b) and J71 : ITIC : O-PDI (1 : 0.9 : 0.1) ternary film (c). Scattering profiles (horizontal and vertical) of J71:ITIC binary film (d), J71 : ITIC : O-PYPDI (1 : 0.9 : 0.1) ternary film (e), and J71 : ITIC : O-PDI (1 : 0.9 : 0.1) ternary film (f).

Published on 29 October 2018. Downloaded by Fail Open on 7/23/2025 8:45:14 AM.

pyrene-fused PDI-NFAs. Additionally, compared to the in-plane lamellar and vertical (out-of-plane) π–π stacking intensity of PDI-NFAs in neat films, pyrene-fused PDI-NFAs show much lower intensity, caused by the twist angle between pyrene and the adjacent PDI unit along with the reduced planarity of the whole molecules. Both neat films of J71 and ITIC exhibit face-on crystallites, as evidenced by the simultaneous appearance of in-plane lamellar stacking and out-of-plane π–π stacking peaks. Similar GIWAXS profiles of the neat J71 film and the binary J71:ITIC film indicate that the molecular arrangement and crystallinity of J71 can be kept well in the blend film (Fig. 6a).

In J71 : ITIC : NFA (1 : 0.9 : 0.1) ternary films, each set of parent PDIs and pyrene-fused PDIs show similar trends, that is, relative to the in-plane lamellar packing intensity of J71:ITIC, J71:ITIC:pyrene-fused PDI-NFAs show slight diminution, while J71:ITIC:PDI-NFAs exhibit distinct diminution (Fig. 6e and f). Taking O-PDI and O-PYPDI as examples, J71:ITIC:O-PYPDI have slightly lower (200) peak compared to J71:ITIC, suggesting that the addition of O-PYPDI suppresses the crystallinity of J71:ITIC as well as weakens charge transport. More obvious diminution of the (200) peak at a similar q value was observed in the J71:ITIC:O-PDI film, revealing its weaker crystallinity than that of J71:ITIC:O-PYPDI. The deteriorating molecular arrangement and crystallinity of J71:ITIC:O-PYPDI and J71:ITIC:O-PDI films can be further confirmed by their declined J_{SC} in ternary OSCs.

Thermal stability

Generally, the stability of OSC devices includes the photochemical and thermal stability, which is significantly important for practical applications.[17] Most studies have focused on the photochemical stability, while investigations on the thermal stability are rarely reported, particularly for those small molecule based OSC devices. Accordingly, thanks to the excellent thermal stability of six NFAs and different morphology of 10% content NFA based ternary films compared to the J71:ITIC binary film, we attempted to explore the thermal stability of ternary active layers with the incorporation of 10% content of NFAs. O-PYPDI and Th-PYPDI based ternary films and host binary films were chosen as the research objects for their good device performance. After spin-coating HTL (PEDOT:PSS) and active layers on the ITO-coated glass substrates in the same way, all substrates were put on a hot plate at 80 °C for different annealing times (12 hours, 24 hours, 48 hours and 72 hours). Then, the PCE test was performed after spin-coating the ETL (PDINO) and vacuum evaporating Al. As shown in Fig. 7a, after annealing for 72 h, the Th-PYPDI and O-PYPDI based devices retained 84% and 82% of their initial PCE values, respectively, while the PCE of the J71:ITIC binary device declined to 75%. The results suggested that both the incorporation of 10% content of Th-PYPDI and O-PYPDI improved the thermal stability of ternary films. In this work, due to the difficulty of measuring the thermal stability of the electron transport layer (PDINO), we investigated the thermal annealing process of the active layer under an inert gas atmosphere. On one hand, the effect of an electrode on the active layer could be excluded,

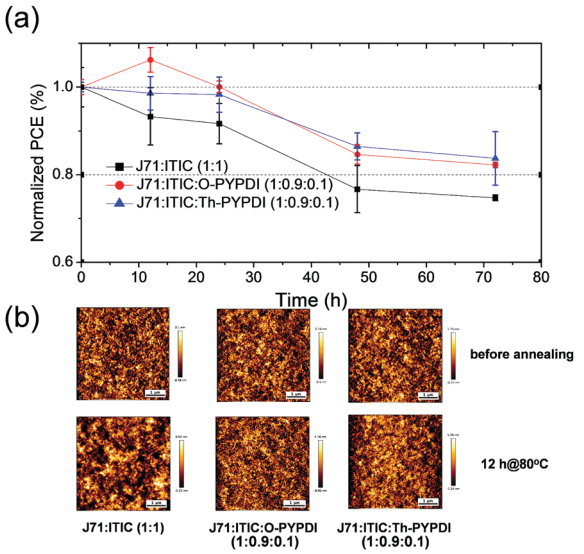

Fig. 7 (a) Stability tests of J71:ITIC binary film, J71 : ITIC : Th-PYPDI (1 : 0.9 : 0.1) and J71 : ITIC : O-PYPDI (1 : 0.9 : 0.1) films stored in the dark at 80 °C. (b) AFM profiles of J71:ITIC binary film, J71 : ITIC : Th-PYPDI (1 : 0.9 : 0.1) and J71 : ITIC : O-PYPDI (1 : 0.9 : 0.1) films before and after annealing for 12 h at 80 °C.

because the electrode had not been heated at 80 °C for 12 h. On the other hand, the effect of oxygen and vapor could be excluded due to the inert gas atmosphere. Therefore, the morphology stability should be the reason for the improved thermal stability of O-PYPDI and Th-PYPDI based ternary films. Thus, to understand the enhanced thermal stability of O-PYPDI and Th-PYPDI based ternary films, AFM measurements of films upon annealing for 12 h at 80 °C were conducted. As shown in Fig. 7b, before annealing, all of the three films display regular and uniform profiles. After annealing, the J71:ITIC binary film exhibited distinct deterioration with a large domain size appearing, and the PCE declined to 93% of the initial value. However, no apparent deterioration was observed in the O-PYPDI and Th-PYPDI based ternary films under the same annealing conditions. The enhanced thermal stability of O-PYPDI and Th-PYPDI based ternary films may be derived from their better morphology stability, in comparison with the J71:ITIC binary film undergoing the same annealing process.

Conclusions

A class of novel pyrene-fused PDI-NFAs were designed to fabricate ternary OSC devices blended with a host J71:ITIC system, which exhibited much better device performances than those of parent PDI counterparts with the same incorporation content. The superior device performance of pyrene-fused PDI-NFA based ternary OSCs should be ascribed to preferable photovoltaic properties, better miscibility and crystallization of the ternary films. The O-PYPDI based ternary device exhibited the best PCE of 10.96% and a good thermal stability with the PCE remaining at 82% of the initial value after thermal annealing at 80 °C for 72 h, demonstrating that pyrene-fused

 This journal is © The Royal Society of Chemistry and the Chinese Chemical Society 2019

Published on 29 October 2018. Downloaded by Fail Open on 7/23/2025 8:45:14 AM.

PDI-NFAs are good candidates for fabrication of ternary OSC devices to improve the absorption in the short wavelength region, V_{OC} and thermal stability.

Conflicts of interest

There are no conflicts to declare.

Acknowledgements

This work was supported by the National Science Foundation of China (no. 51573140, 21734007, 21702154, and 51773157), Hubei Province (2017CFA002), and Special funds for basic scientific research services in central colleges and Universities (2042017kf0247). This work was performed in part on the SAXS/WAXS beamline at the Australian Synchrotron, part of ANSTO.

Notes and references

1 (*a*) L. X. Meng, Y. M. Zhang, X. J. Wan, C. X. Li, X. Zhang, Y. B. Wang, X. Ke, Z. Xiao, L. M. Ding, R. X. Xia, H. L. Yip, Y. Cao and Y. S. Chen, *Science*, 2018, **361**, 1094; (*b*) P. Cheng, G. Li, X. W. Zhan and Y. Yang, *Nat. Photonics*, 2018, **12**, 131–142; (*c*) J. Q. Zhang, H. S. Tan, X. G. Guo, A. Facchetti and H. Yan, *Nat. Energy*, 2018, **3**, 720–731; (*d*) Y. Z. Lin, Y. F. Li and X. W. Zhan, *Chem. Soc. Rev.*, 2012, **41**, 4245; (*e*) Y. Z. Lin and X. W. Zhan, *Mater. Horiz.*, 2014, **1**, 470; (*f*) A. Gupta, A. Rananaware, P. S. Rao, D. D. La, A. Bilic, W. C. Xiang, J. L. Li, R. A. Evans, S. V. Bhosalec and S. V. Bhosale, *Mater. Chem. Front.*, 2017, **1**, 1600; (*g*) A. Rananaware, A. Gupta, G. Kadam, D. D. La, A. Bilic, W. C. Xiang, R. A. Evansf and S. V. Bhosale, *Mater. Chem. Front.*, 2017, **1**, 2511; (*h*) F. Yang, C. Li, W. B. Lai, A. D. Zhang, H. Huang and W. W. Li, *Mater. Chem. Front.*, 2017, **1**, 1389; (*i*) J. C. Jia, N. N. Zheng, Z. F. Wang, Y. P. Huang, C. H. Duan, F. Huang and Y. Cao, *Sci. China: Chem.*, 2017, **60**, 1458; (*j*) H. T. Zhang, Y. T. Liu, Y. N. Sun, M. M. Li, W. Ni, Q. Zhang, X. J. Wan and Y. S. Chen, *Sci. China: Chem.*, 2017, **60**, 366; (*k*) J. Q. Xu, W. Q. Liu, S. Y. Liu, J. Ling, J. Q. Mai, X. H. Lu, C. Z. Li, A. K.-Y. Jen and H. Z. Chen, *Sci. China: Chem.*, 2017, **60**, 561; (*l*) J. H. Hou, O. Inganäs, R. H. Friend and F. Gao, *Nat. Mater.*, 2018, **17**, 119.

2 (*a*) C. Q. Yan, S. Barlow, Z. H. Wang, H. Yan, A. K.-Y. Jen, S. R. Marder and X. W. Zhan, *Nat. Rev. Mater.*, 2018, **3**, 18003; (*b*) Z. Y. Li, S. X. Dai, J. M. Xin, L. Zhang, Y. Wu, J. Rech, F. W. Zhao, T. F. Li, K. Liu, Q. Liu, W. Ma, W. You, C. R. Wang and X. W. Zhan, *Mater. Chem. Front.*, 2018, **2**, 537; (*c*) L. Feng, C. Wang, X. Y. Deng, X. C. Miao, J. Q. Wang, Y. Y. Wang and Z. Li, *Mater. Chem. Front.*, 2018, **2**, 264; (*d*) C. Zhang, T. Liu, W. X. Zeng, D. J. Xie, Z. H. Luo, Y. M. Sun and C. L. Yang, *Mater. Chem. Front.*, 2017, **1**, 749; (*e*) W. Y. Liu, Z. C. Zhou, T. Vergote, S. J. Xu and X. Z. Zhu, *Mater. Chem. Front.*, 2017, **1**, 2349; (*f*) X. J. Long, Z. C. Ding, C. D. Dou, J. Liu and L. X. Wang, *Mater. Chem. Front.*, 2017, **1**, 852; (*g*) L. Lv, X. F. Wang, T. Dong, X. L. Wang, X. X. Wu, L. Yang and H. Huang, *Mater. Chem. Front.*, 2017, **1**, 1317.

3 (*a*) N. S. Saricifci, L. Saricifci, A. J. Heeger and F. Wudl, *Science*, 1992, **258**, 1474; (*b*) J. E. Anthony, A. Facchetti, M. Heeney, S. R. Marder and X. Zhan, *Adv. Mater.*, 2010, **22**, 3876; (*c*) Y. He and Y. Li, *Phys. Chem. Chem. Phys.*, 2011, **13**, 1970.

4 (*a*) A. a. F. Eftaiha, J.-P. Sun, I. G. Hill and G. C. Welch, *J. Mater. Chem. A*, 2014, **2**, 1201; (*b*) P. Sonar, J. P. Fong Lim and K. L. Chan, *Energy Environ. Sci.*, 2011, **4**, 1558.

5 (*a*) G. Y. Zhang, J. B. Zhao, P. C. Y. Chow, K. Jiang, J. Q. Zhang, Z. L. Zhu, J. Zhang, F. Huang and H. Yan, *Chem. Rev.*, 2018, **118**, 3447; (*b*) W. Q. Chen and Q. C. Zhang, *J. Mater. Chem. C*, 2017, **5**, 1275; (*c*) N. N. Liang, W. Jiang, J. H. Hou and Z. H. Wang, *Mater. Chem. Front.*, 2017, **1**, 1291; (*d*) S. X. Dai, S. M. Zhang, Q. D. Ling and X. W. Zhan, *Chin. J. Polym. Sci.*, 2017, **35**, 230; (*e*) A. Islama, Z. Y. Liu, R. X. Peng, W. G. Jiang, T. Lei, W. Li, L. Zhang, R. J. Yang, Q. Guan and Z. Y. Ge, *Chin. J. Polym. Sci.*, 2017, **35**, 171.

6 (*a*) G. P. Gao, N. N. Liang, H. Geng, W. Jiang, H. T. Fu, J. J. Feng, J. H. Hou, X. L. Feng and Z. H. Wang, *J. Am. Chem. Soc.*, 2017, **139**, 15914; (*b*) Y. W. Duan, X. Q. Xu, H. Yan, W. L. Wu, Z. J. Li and Q. Peng, *Adv. Mater.*, 2017, **29**, 1605115; (*c*) D. Meng, H. T. Fu, C. Y. Xiao, X. Y. Meng, T. Winands, W. Ma, W. Wei, B. B. Fan, L. J. Huo, N. L. Doltsinis, Y. Li, Y. M. Sun and Z. H. Wang, *J. Am. Chem. Soc.*, 2016, **138**, 10184; (*d*) J. Liu, S. S. Chen, D. P. Qian, B. Gautam, G. F. Yang, J. B. Zhao, J. Bergqvist, F. L. Zhang, W. Ma, H. Ade, O. Inganäs, K. Gundogdu, F. Gao and H. Yan, *Nat. Energy*, 2016, **1**, 16089; (*e*) L. Yang, W. X. Gu, L. Lv, Y. S. Chen, Y. F. Yang, P. Ye, J. F. Wu, L. Hong, A. D. Peng and H. Huang, *Angew. Chem., Int. Ed.*, 2018, **57**, 1096; (*f*) T. J. Sisto, Y. Zhong, B. Y. Zhang, M. T. Trinh, K. Miyata, X. J. Zhong, X. Y. Zhu, M. L. Steigerwald, F. Ng and C. Nuckolls, *J. Am. Chem. Soc.*, 2017, **139**, 5648; (*g*) H. Chang, Z. M. Chen, X. Y. Yang, Q. W. Yin, J. Zhang, L. Ying, X. F. Jiang, B. M. Xu, F. Huang and Y. Cao, *Org. Electron.*, 2017, **45**, 227.

7 J. Q. Zhang, Y. K. Li, J. C. Huang, H. W. Hu, G. Y. Zhang, T. X. Ma, P. C. Y. Chow, H. Ade, D. Pan and H. Yan, *J. Am. Chem. Soc.*, 2017, **139**, 16092.

8 X. J. Zhan, W. T. Xiong, Y. B. Gong, T. Liu, Y. J. Xie, Q. Peng, Y. M. Sun and Z. Li, *Sol. RRL*, 2017, **1**, 1700123.

9 (*a*) X. Y. Liu, Y. J. Yan, Y. Yao and Z. Q. Liang, *Adv. Funct. Mater.*, 2018, **28**, 1802004; (*b*) M. Zhang, W. Gao, F. J. Zhang, Y. Mi, W. B. Wang, Q. S. An, J. Wang, X. L. Ma, J. L. Miao, Z. H. Hu, X. F. Liu, J. Zhang and C. L. Yang, *Energy Environ. Sci.*, 2018, **11**, 841; (*c*) Z. Xiao, X. Jia and L. M. Ding, *Sci. Bull.*, 2017, **62**, 1562; (*d*) L. Y. Lu, W. Chen, T. Xu and L. P. Yu, *Nat. Commun.*, 2015, **6**, 7327; (*e*) H. Li, Z. Xiao, L. M. Ding and J. Z. Wang, *Sci. Bull.*, 2018, **63**, 340; (*f*) H. Lu, J. C. Zhang, J. Y. Chen, Q. Liu, X. Gong, S. Y. Feng, X. J. Xu, W. Ma and Z. S. Bo, *Adv. Mater.*, 2016, **28**, 9559; (*g*) L. Zhang and W. Ma, *Chin. J. Polym. Sci.*, 2017, **35**, 184.

Published on 29 October 2018. Downloaded by Fail Open on 7/23/2025 8:45:14 AM.

10 (*a*) Y. S. Chen, P. Ye, Z. G. Zhu, X. L. Wang, L. Yang, X. Z. Xu, X. X. Wu, T. Dong, H. Zhang, J. H. Hou, F. Liu and H. Huang, *Adv. Mater.*, 2017, **29**, 1603154; (*b*) T. Liu, Y. Guo, Y. P. Yi, L. J. Huo, X. N. Xue, X. B. Sun, H. T. Fu, W. T. Xiong, D. Meng, Z. H. Wang, F. Liu, T. P. Russell and Y. M. Sun, *Adv. Mater.*, 2016, **28**, 10008; (*c*) K. Jiang, G. Y. Zhang, G. F. Yang, J. Q. Zhang, Z. K. Li, T. X. Ma, H. W. Hu, W. Ma, H. Ade and H. Yan, *Adv. Energy Mater.*, 2018, **8**, 1701370.

11 (*a*) X. L. Ma, W. Gao, J. S. Yu, Q. S. An, M. Zhang, Z. H. Hu, J. X. Wang, W. H. Tang, C. L. Yang and F. J. Zhang, *Energy Environ. Sci.*, 2018, **11**, 2134; (*b*) Y. P. Xie, F. Yang, Y. X. Li, M. A. Uddin, P. Q. Bi, B. B. Fan, Y. H. Cai, X. T. Hao, H. Y. Woo, W. W. Li, F. Liu and Y. M. Sun, *Adv. Mater.*, 2018, 1803045.

12 (*a*) Y. B. Gong, P. Zhang, Y. R. Gu, J. Q. Wang, M. M. Han, C. Chen, X. J. Zhan, Z. L. Xie, B. Zou, Q. Peng, Z. G. Chi and Z. Li, *Adv. Opt. Mater.*, 2018, **6**, 1800198; (*b*) X. J. Zhan, J. Zhang, Y. B. Gong, S. Tang, J. Tu, Y. Xie, Q. Peng, G. Yu and Z. Li, *Mater. Chem. Front.*, 2017, **1**, 2341; (*c*) Y. B. Gong, X. J. Zhan, Q. Q. Li and Z. Li, *Sci. China: Chem.*, 2016, **59**, 1623; (*d*) X. Zhan, J. Zhang, S. Tang, Y. X. Lin, M. Zhao, J. Yang, H. L. Zhang, Q. Peng, G. Yu and Z. Li, *Chem. Commun.*, 2015, **51**, 7156.

13 Y. Z. Lin, J. Y. Wang, Z. G. Zhang, H. T. Bai, Y. F. Li, D. B. Zhu and X. W. Zhan, *Adv. Mater.*, 2015, **27**, 1170.

14 H. J. Bin, L. Gao, Z. G. Zhang, Y. K. Yang, Y. D. Zhang, C. F. Zhang, S. S. Chen, L. W. Xue, C. D. Yang, M. Xiao and Y. F. Li, *Nat. Commun.*, 2016, **7**, 13651.

15 (*a*) P. P. Khlyabich, A. E. Rudenko, R. A. Street and B. C. Thompson, *ACS Appl. Mater. Interfaces*, 2014, **6**, 9913; (*b*) N. S. Gobalasingham, S. T. Noh, J. B. Howard and B. C. Thompson, *ACS Appl. Mater. Interfaces*, 2016, **8**, 27931.

16 S. Wu, *J. Polym. Sci., Part C: Polym. Lett.*, 1971, **34**, 19.

17 (*a*) K. Zhang, R. X. Xia, B. B. Fan, X. Liu, Z. F. Wang, S. Dong, H. L. Yip, L. Ying, F. Huang and Y. Cao, *Adv. Mater.*, 2018, 1803166; (*b*) D. Baran, R. S. Ashraf, D. A. Hanifi, M. Abdelsamie, N. Gasparini, J. A. Röhr, S. Holliday, A. Wadsworth, S. Lockett, M. Neophytou, C. J. M. Emmott, J. Nelson, C. J. Brabec, A. Amassian, A. Salleo, T. Kirchartz, J. R. Durrant and I. McCulloch, *Nat. Mater.*, 2017, **16**, 4797; (*c*) D. Landerer, A. Mertens, D. Freis, R. Droll, T. Leonhard, A. D. Schulz, D. Bahro and A. Colsmann, *npj Flexible Electron.*, 2017, **11**, 1; (*d*) Z. Wang, H. Y. Jiang, L. J. Zhang, X. C. Liu, J. M. Sun, Y. Cao and J. W. Chen, *Org. Electron.*, 2018, **61**, 359; (*e*) X. Y. Du, T. Heumueller, W. Gruber, A. Classen, T. Unruh, N. Li and C. J. Brabec, *Joule*, DOI: 10.1016/j.joule.2018.09.001.

 This journal is © The Royal Society of Chemistry and the Chinese Chemical Society 2019